PCCP

PAPER

View Article Online
View Journal | View Issue

Cite this: *Phys. Chem. Chem. Phys.*, 2019, **21**, 6101

Laser and electron beam-induced formation of Ag/Cr structures on Ag_2CrO_4†

Lemos P. S.,[a] Silva G. S.,[a] Roca R. A.,[a] Assis M.,[a] Torres-Mendieta R.,[b] Beltrán-Mir H.,[c] Mínguez-Vega G.,[d] Cordoncillo E.,[c] Andrés J.[e] and Longo E.*[f]

Received 26th November 2018,
Accepted 7th February 2019

DOI: 10.1039/c8cp07263a

rsc.li/pccp

The interactions of silver chromate (Ag_2CrO_4) with a femtosecond (fs) laser and electron beam irradiations were investigated. For the first time, the growth and coalescence of metallic Ag nanoparticles (NPs) on an Ag_2CrO_4 surface *via* fs laser irradiation can be reported. Furthermore, electron beam irradiation causes a segregation process of Ag NPs in which Ag nanofilaments are obtained. The Ag_2CrO_4 particles were characterized using X-ray diffraction (XRD), micro-Raman spectroscopy (Raman), field-emission scanning electron microscopy (FE-SEM), high-resolution electron microscopy, and energy-dispersive X-ray spectroscopy (EDS). According to the results, the fs/electron beam irradiations of Ag_2CrO_4 are environmentally friendly, fast, and effective methods to produce metallic Ag NPs. Both strategies have enormous potential for the synthesis and morphological control of Ag NPs on templates or biotemplates, core–shells, decorations, and composites based on $Ag_{2-x}CrO_4$:Ag materials, which are difficult to synthesize using conventional chemical and physical methods.

Introduction

Nanoscale-manipulations of atoms are possible through the ever-increasing advances of modern technologies, such as electron microscopy[1,2] and ultra-short laser radiation,[3] which open up a number of exciting possibilities for the nanoscale-controlled *in situ* fabrication of nanoparticles (NPs). When a material is subjected to external perturbation, *e.g.*, an electron beam or femtosecond (fs) pulse laser irradiation, a large amount of energy is interchanged through nonequilibrium processes, thereby altering the geometry, electronic structure, and morphology of the irradiated material.[4–7] These changes cause unexpected effects on their physical and chemical properties, *e.g.*, photoluminescence emission,[8] photodegradation,[9] antimicrobial activity,[10] and the growth of nanostructures.[10,11] Excellent studies have been published on electron beam-induced syntheses[12,13] and how different functional nanomaterials and nanostructures have been successfully fabricated using fs laser treatment for several practical applications.[3,14–19] Both techniques have gained enormous attention owing to their ability to investigate the structure–property relation of nanomaterials and their chemical interactions with solid surfaces.

Recently, fs laser and electron beam irradiation have been widely employed to grow metallic NPs of Ag,[20–29] Au NPs,[30–32] Bi NPs,[33,34] Os NPs,[35] Cu NPs,[36,37] Pt NPs,[38] Li NPs,[39] Na NPs,[40] Mg NPs,[41] Ca NPs,[42] and Ba NPs.[41] Moreover, electron beam and fs laser irradiation do not require the addition of any solvent or chemistry component during the formation process of nanostructures. Thus, these techniques can be considered as environmentally friendly according to the principles of green chemistry[43] and the resulting nanomaterials could be applied to a wide range of technological applications.

Our research group investigates Ag-containing semiconductors that have attracted significant attention owing to their rich history in technical applications, *e.g.*, in catalysis,[44] photocatalysis,[45] for gas sensors,[46] and antimicrobial agents.[45] In this context, a variety of Ag-containing oxides such as Ag_2WO_4 in their different polymorph forms α–Ag_2WO_4,[20] β–Ag_2WO_4,[21,47] and γ–Ag_2WO_4[48] have been studied. Various Ag-based compounds such as β-Ag_2MoO_4,[49] Ag_3PO_4,[50,51] β-$AgVO_3$,[52] and Ag_2CrO_4[53] have shown the ability to form Ag NPs under electron beam irradiation. The Ag NPs' growth on the semiconductor templates could enhance the surface plasmon resonance effect, which can dramatically amplify the absorption of visible light

[a] *INCTMN-CDMF, Universidade Federal de São Carlos, P.O. Box 676, 13565-905 São Carlos, SP, Brazil*
[b] *Institute for Nanomaterials, Advanced Technologies and Innovation, Technical University of Liberec, Studentská 1402/2, 461 17 Liberec, Czech Republic*
[c] *Department of Inorganic and Organic Chemistry, University Jaume I (UJI), Castelló 12071, Spain*
[d] *GROC UJI, Institut de Noves Tecnologies de la Imatge (INIT), University Jaume I (UJI), Castelló 12071, Spain*
[e] *Department of Analytical and Physical Chemistry, University Jaume I (UJI), Castelló 12071, Spain*
[f] *INCTMN-UNESP, Universidade Estadual Paulista, P.O. Box 355, 14801-907 Araraquara, SP, Brazil*

† Electronic supplementary information (ESI) available. See DOI: 10.1039/c8cp07263a

and improve the separation rate of the photogenerated holes and electrons, thereby enhancing the photocatalytic activity.[54] In this context, recently, we have presented the scale-up of the formation of Ag NPs on α-Ag_2WO_4 with bactericidal properties *via* fs laser irradiation,[55] the laser-induced formation of Bi NPs with different crystallographic structures,[56] and the formation of In NPs provoked by laser/electron beam irradiation.[57]

In the current work, the semiconductor under study is Ag_2CrO_4, which is a promising inorganic material because of its unique electronic and crystal structure that enables it to be a good photocatalyst.[58–65] Our group performed the synthesis, characterization, and determination of the photoluminescence properties of Ag_2CrO_4 microcrystals.[66] In addition, the formation and growth of Ag NPs on Ag_2CrO_4 induced by electron irradiation on an electron microscope was investigated.[53] It is well known that the photo- and electrochemical properties of semiconductor films used in photovoltaics, photocatalysis, and photoelectrolysis are greatly enhanced by the deposition of Ag NPs onto their surfaces. The Ag NPs are employed as a high visible-light-driven photocatalyst and microbial agent[10,49,50,52,67] to enhance the performance. The improved properties appear owing to the surface plasmon resonance (SPR) effect and extended visible-light absorption that is present in metallic Ag NPs. Hence, a plasmon band is created, the charge recombination reduced, and their response improved.[68,69] This study is intended to complement our previous studies. The goal is two-fold: (i) to demonstrate, for the first time, that fs laser irradiation can be used for the formation of Ag NPs on Ag_2CrO_4 surfaces, and (ii) to study the evolution behavior and growth mechanisms of Ag NPs induced by electron beam and fs laser irradiation.

Experimental

Synthesis of Ag_2CrO_4 microparticles

Two Ag_2CrO_4 samples were synthesized using the precipitation method without any surfactants. The chromate precursor solution was prepared in 50 mL of distilled water, to which 1.0×10^{-3} mol of K_2CrO_4 was added (99.5% purity; Química Especializada Erich Ltda–QEEL). The solution was magnetically stirred until it turned homogeneous and yellow. The silver precursor solution was prepared with 2.0×10^{-3} mol of $AgNO_3$ (99.8% purity; Alfa Aesar) in 50 mL distilled water. The solution was magnetically stirred until it turned homogeneous and transparent. The addition of the silver precursor solution to the chromate precursor solution was carried out with dropwise additions with a rate of 10 mL min^{-1}. The resultant solution was magnetically stirred for 20 minutes. The precipitate was washed four times with water and once with acetone and afterward dried in a stove at 60 °C for 4 hours.

Structural characterization of Ag_2CrO_4 microparticles

The Ag_2CrO_4 was structurally characterized by X-ray diffraction (XRD) using a D/MAX-2500 PC diffractometer (Rigaku) with Cu Kα radiation (λ = 1.5406 Å). The data were recorded in the normal routine for 2θ values ranging from 15° to 60° with a scanning velocity of 2° min^{-1}. Micro-Raman measurements were conducted using an iHR550 spectrometer (Horiba Jobin Yvon, Japan) coupled to a CCD detector and an Ag ion laser (MellesGriot, USA) operating at 514.5 nm with a maximum power of 200 mW and a fiber microscope. The measurements were performed in the range of 30–1000 cm^{-1}.

Fs laser irradiation

To perform the fs laser irradiation, the sample had to be compressed into a pellet form. The resulting Ag_2CrO_4 pellets were irradiated with a Ti:sapphire laser (Femtopower Compact Pro, Femtolasers), which delivers 30 fs full-width at half-maximum (FWHM) pulses at a central wavelength of 800 nm and a repetition rate of 1 kHz. In addition, a programmable acousto-optic filter (Dazzler, Fastlite) was used to ensure a precise pulse compression at the sample. A laser beam with a mean power of 200 mW was focused onto the surface of the pellet target with a 75 mm lens to obtain a focal spot with a diameter of 20.6 μm FWHM. The silver chromate sample was placed at the top of a quartz slide attached to a two-dimensional motion-controlled stage moving at a constant speed of 0.45 mm s^{-1} in the focus plane perpendicular to the laser beam. Fig. 1a and b present a scheme of the experimental procedure and obtained results, where the interaction between the fs laser radiation and Ag_2CrO_4 promotes the creation of a plasma plume that leads to the segregation of Ag nanoparticles. The selected parameters of the laser irradiation are similar to those previously reported for the most efficient segregation of metal NPs from semiconductor networks.[55–57] In addition, when we are dealing with pulsed laser sources that interact with a moving target, as the light is not delivered in a continuous way, it is more common to talk about the overlapping between the pulses on the sample. In this way, a large overlap means more investment of energy delivered to a single area in a long period of time, and a minimal overlap means a minor investment of energy delivered to a single area but in a short period of time. For the current experiment, the irradiation time is controlled by the size of the beam and the speed of the platform. The size of the focal spot on the sample surface was about 20.7 microns. The laser has a 1 KHz repetition rate and the motion velocity of the platform was 0.45 mm s^{-1}. These parameters indicate that there is an overlapping of the spot size of around 95% between consecutive pulses. Considering the large overlapping used in the current experiment, in comparison with electron beam excitation, while using fs laser irradiation there is still plenty of room towards crossing the line between basic research and the final industrialization of the process.

Morphological characterization of the samples

The morphology of fs laser-irradiated and non-irradiated samples was observed using a field-emission scanning electron microscope (FE-SEM) (Inspect F50 model; FEI Company, USA) working at 5 kV. Transmission electron microscopy (TEM) images are obtained using a high-resolution (HR) JEM-2100 LaB6 (Jeol) microscope with an acceleration voltage of 200 kV coupled with INCA Energy TEM 200 (Oxford Instruments) to perform

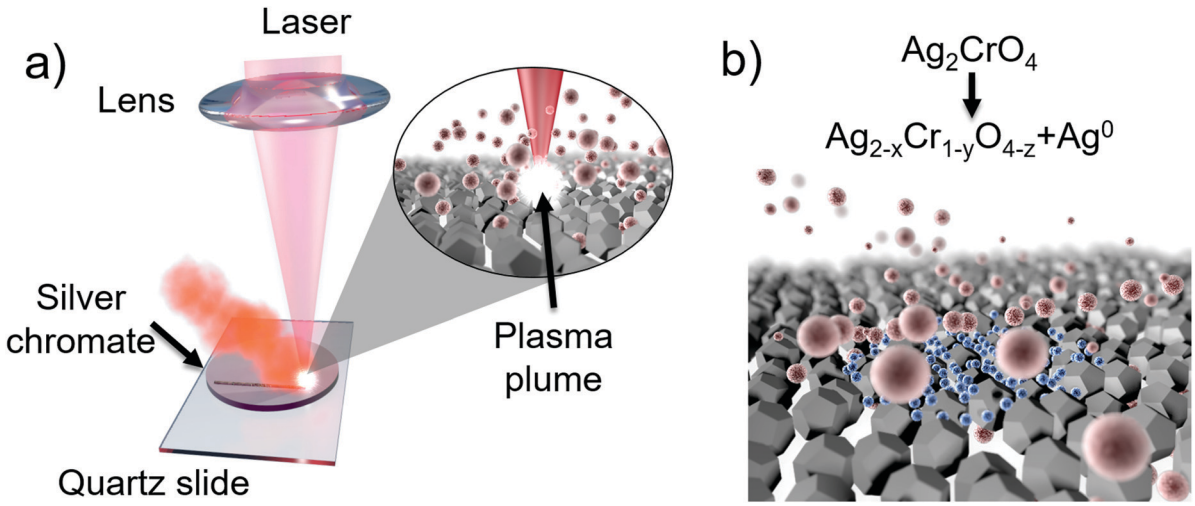

Fig. 1 Representation of the procedure employed to irradiate Ag_2CrO_4, where the generation of the plasma plume takes place (left), with formation of $Ag_{2-x}CrO_4$:Ag (right). (a) Experimental procedure and (b) schematic representation of the obtained results.

energy-dispersive X-ray spectroscopy (EDS). For both the non-laser irradiated powder and the laser irradiated powder, in the case of FE-SEM, the samples were prepared by depositing a small amount of powder directly onto the FE-SEM sample holder, and for the TEM the powder was suspended in water and a droplet of the mixture was deposited onto the carbon-coated Cu grid (TEM grid). After the evaporation of water, it was submitted to high vacuum and analyzed *via* TEM.

Results and discussion

XRD patterns

Fig. 2 presents the XRD patterns of the Ag_2CrO_4 microparticles prepared using the aforementioned methodology. All diffraction peaks can be perfectly indexed to an orthorhombic structure with space group *Pnma* and without any deleterious phases within the detection limits of the diffractometer. The well-defined peaks indicate long-range structural order and crystallinity. The XRD patterns are in good agreement with the *Inorganic Crystal Structure Database* (ICSD) Card no. 16298 and literature.[53,70]

Fig. 3 illustrates the orthorhombic structure of the Ag_2CrO_4 microparticles. The figure is produced using the *Visualization for Electronic and Structural Analysis* (VESTA) program, version 3.3.2., using lattice parameters and atomic positions obtained from the crystallographic information file (CIF) no. 16298.

According to Silva *et al.*,[66] the Ag_2CrO_4 structure is composed of elongated octahedral [AgO_6] clusters and distorted off-centered [AgO_4] tetrahedra and [CrO_4] clusters. The tetrahedral clusters interact with the octahedral [AgO_6] ones, generating polarization at the short and medium distance, which is reflected throughout the crystalline lattice. These structural and electronic displacements promote the formation of induced and permanent dipoles between the different clusters,

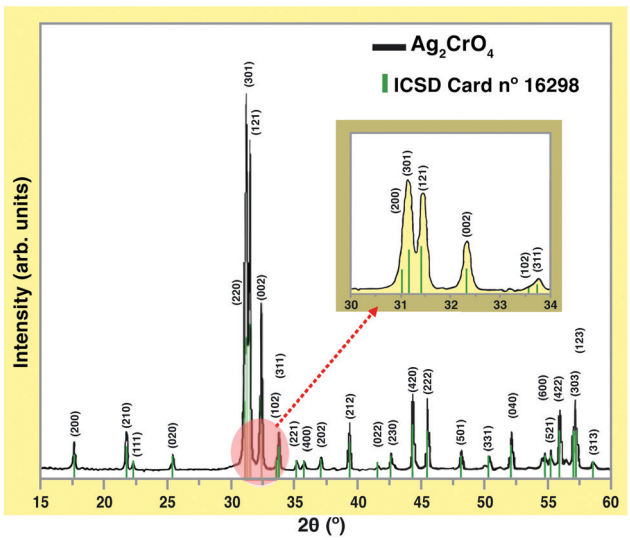

Fig. 2 XRD pattern of the non-irradiated Ag_2CrO_4 microcrystals.

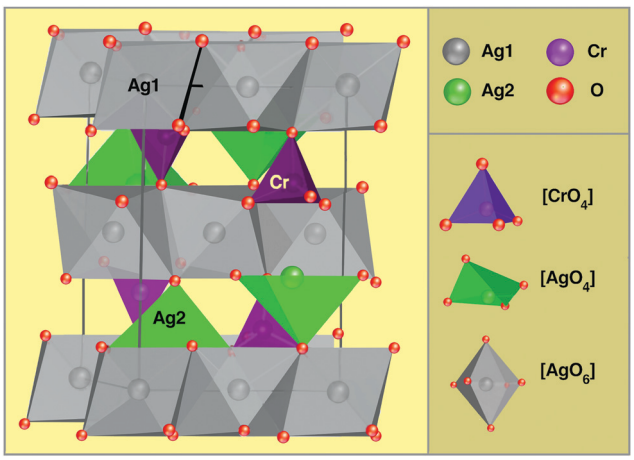

Fig. 3 A schematic representation of the orthorhombic structure of Ag_2CrO_4 microparticles. The [CrO_4], [AgO_4] and [AgO_6] clusters, as building blocks of Ag_2CrO_4, are depicted.

enhancing domains of different electron density distributions (low and high) in the crystalline network.[71]

Raman spectra

Furthermore, a micro-Raman analysis was performed to investigate the degree of structural order–disorder in the short-range (Fig. 4). The micro-Raman spectrum presents three peaks in the high-frequency region at 781, 812, and 855 cm^{-1}. These peaks are related to the symmetric stretching vibrations of Cr–O bonds in the [CrO_4] clusters and their positions are in good agreement with the literature.[72] The orthorhombic structure of Ag_2CrO_4 has 36 Raman-active modes with mechanical representation Γ = 11A_g + 7B1$_g$ + 11B2$_g$ + 7B3$_g$, of which 18 are internal modes [2ν_1, 4ν_2, 6ν_3, 6ν_4] and 18 are external modes [6 rotational (R) and 12 translational (T) modes].[53] Not all Raman-active modes were experimentally observed owing to weak intensity and/or merging of modes with close wavenumbers.

FE-SEM images

To investigate the morphological alterations resulting from the fs laser irradiation, FE-SEM micrographs were analyzed. The non-irradiated particles present a high agglomeration rate when observed under low magnification (Fig. 5a). However, when these particles are analyzed at medium and high magnifications (Fig. 5b and c), they appear faceted and formed mainly by irregular polyhedrons. The particles of the fs laser-irradiated sample (Fig. 5d–f) are faceted and present irregular polyhedra (slightly different from those observed in the non-irradiated sample).

To analyze the effects of fs laser irradiation on the morphology and the particle size distribution more deeply, a count of 200 particles of each sample was taken, and the results are presented in Fig. 6. The distribution curve in each histogram, the mean height, and the width of the particles were calculated using a log-normal distribution curve. The non-irradiated sample (Fig. 6a and b) showed a very narrow particle size distribution.

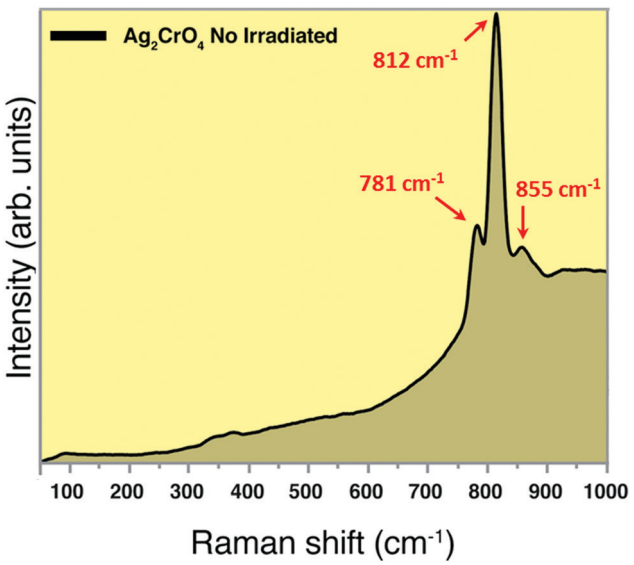

Fig. 4 Raman scattering spectrum of the non-irradiated Ag_2CrO_4 sample.

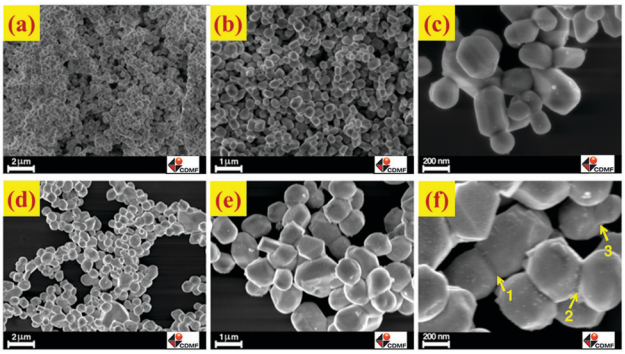

Fig. 5 (a) Low-, (b) medium-, and (c) high-magnifcation FE-SEM images of the non-irradiated Ag_2CrO_4 sample. (d) Low-, (e) medium-, and (f) high-magnification FE-SEM images of the fs laser-irradiated Ag_2CrO_4 sample. *Numbers 1, 2 and 3 in (f) indicate the initial stage of the sintering process.

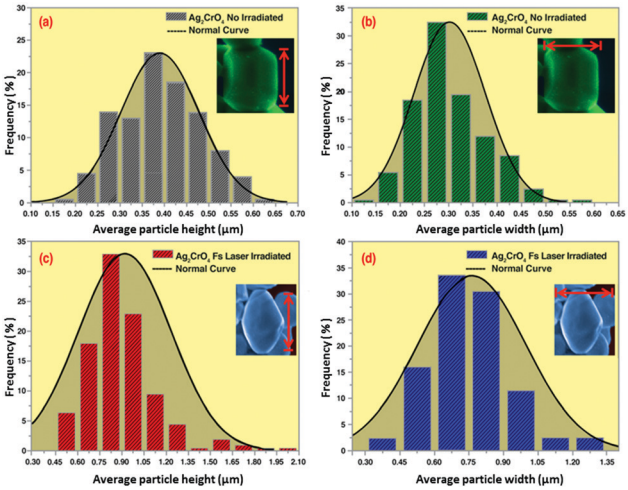

Fig. 6 Average height and width distribution of Ag_2CrO_4 microparticles non-irradiated (a and b) and fs laser-irradiated (c and d).

The particles have a size distribution range between 0.10 µm and 0.60 µm. In addition, the non-irradiated particles exhibit a mean height and a width of (0.39 ± 0.09) µm and (0.30 ± 0.07) µm, respectively. On the other hand, the fs laser-irradiated sample (Fig. 6c and d) presented a particle size distribution ranging from 0.45 µm to more than 2.0 µm, and a mean height and a width of (0.92 ± 0.31) µm and (0.76 ± 0.24) µm, respectively. These values show that a significant increase in the particle size distribution of the fs laser-irradiated sample relative to the non-irradiated sample has occurred. The results reveal that the coalescence process has taken place and that the particles' growth has been stimulated by fs laser-irradiation.

By plotting the height of each particle with its own width (Fig. 7), a considerable increase in the dispersion of particles from the non-irradiated to fs laser-irradiated samples can be observed. In addition, the width/height ratios of the particles are similar (0.77 for the non-irradiated particles and 0.83 for the irradiated particles), which suggests that the coalescence process did not occur along a preferable unidirectional orientation or oriented attachment.[73]

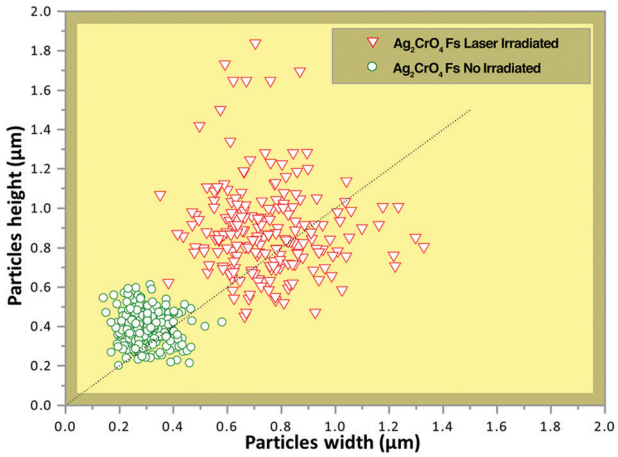

Fig. 7 Height *versus* width of non-irradiated Ag_2CrO_4 particles (green circles) and height *versus* width of fs laser-irradiated Ag_2CrO_4 particles (red triangles).

The coalescence process could be observed using microscopes. In Fig. 5f, the numbers 1, 2, and 3 present the neck growth between contacting particles, which indicate an early stage of the sintering process.[74] As other groups have previously reported, the interaction between high intensity fs laser radiation and a semiconductor powder may promote a microsintering process.[75] The whole interaction can be thought to occur in three stages: In the first stage, the laser irradiation promotes the detachment of electrons, ions and another bigger species out of the surface of the microparticles that interact with the laser radiation, leading to the creation of a plasma plume. In the second stage, there is no more interaction with the laser because the temporal width of the pulses used in the current article is 30 fs, but in the counterpart, the plasma plume still exists (lifetime in the region of ns), which interacts with the remaining powder bed. The plasma plume can reach extremely high temperature and pressure values, 1000 K and 10^{10} Pa, respectively.[76] As the melting temperature of Ag_2CrO_4 is around 938 K,[77] such conditions can promote the melting of the microparticles in the powder bed that interact with the plasma.

In the third stage, the plasma plume gets extinguished and the species that formed the plasma plume cool down and form nanostructures, and the melted microparticles belonging to the powder bed also cool down and solidify forming bigger microparticles. A graphical representation of these stages can be found in the ESI.†

HR-TEM images

In order to investigate the effects of fs laser irradiation on the nanostructure growth and stoichiometric modifications of the original material, HR-TEM images were analyzed. Fig. 8 depicts a representative micrograph of the laser-treated samples. Four different regions are highlighted. Region (b) shows a zoomed-in particle near the stems. Through the zoom, it was possible to examine the lattice planes, which show that the reciprocal distances corresponding to the strongest reflections have the diffraction index (111). This matches with Ag according to the *Joint Committee on Powder Diffraction Standards* (JCPDS) No. 65-2871. Region (c) corresponds to the stems formed *via* fs laser irradiation. The EDS spectra indicate that this region exhibits 80.6% of Ag, 1.8% of Cr and 17.6% of O in its atomic composition. By contrast, region (d) exhibits only the presence

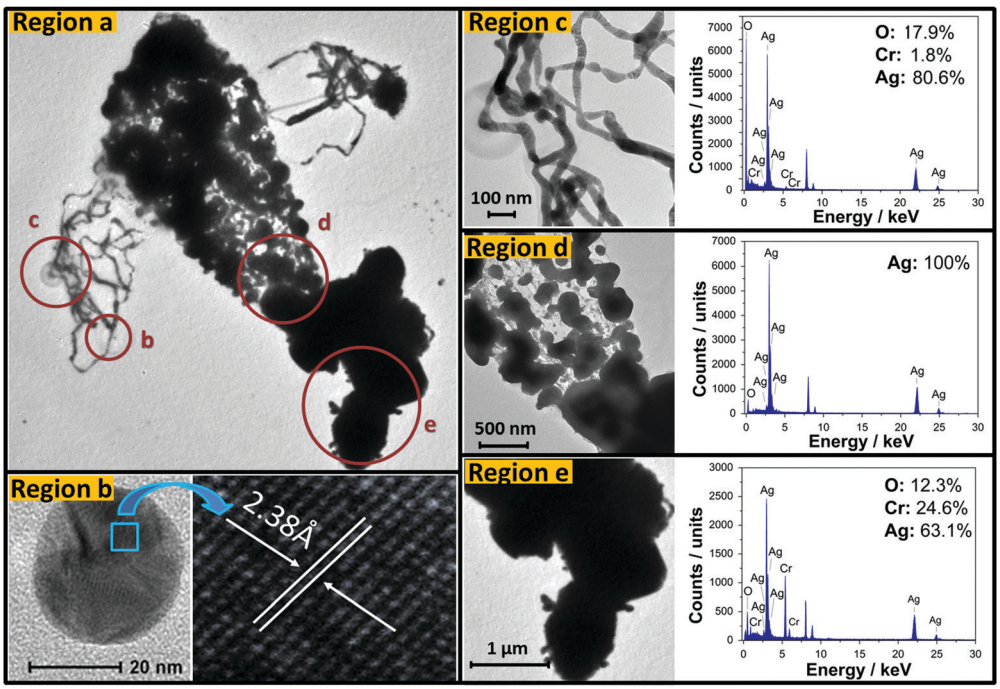

Fig. 8 (Region a) TEM images of the Ag_2CrO_4 microparticles irradiated with fs laser, (Region b) high resolution of the structure formed by fs laser radiation, (Region c) EDS characterization of the stems, (Region d) EDS characterization between the stems and the Ag_2CrO_4 microparticle and (Region e) EDS characterization of the Ag_2CrO_4 microparticle.

of Ag (100%). Region (e) shows the lowest concentration of Ag (63.1%) and the highest concentration of Cr (24.6%). After a conversion of the elementary percentages into molar fractions to estimate the stoichiometry of the material, we noticed that in all regions, the stoichiometric coefficients do not match the Ag_2CrO_4 coefficients. These results suggest that in addition to metallic silver, fs laser-irradiation may form other products, such as simple metal oxides of silver (Ag_wO_x) and chromium (Cr_yO_z).

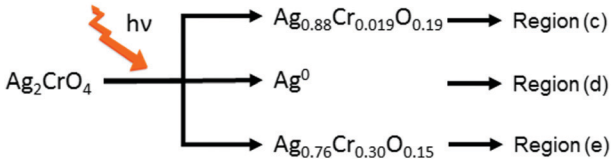

The morphology of the sample irradiated by the fs laser remained unchanged during the observation *via* TEM. This indicates that the stem growth is a consequence of the interactions between the sample and the fs laser irradiation. Since the fs laser-irradiated sample remained unchanged during the presence of the electron beam of the TEM, it can be assumed that the stems are thermodynamically stable because the sample received inside the TEM high-vacuum chamber energy doses of the order of 1.2×10^8 kJ m^{-2}, which would be more than sufficient to alter the sample previously irradiated with the fs laser.

According to the EDS measurements (Fig. 8) the fs laser irradiation provokes the formation of $Ag_{2-x}Cr_{1-y}O_{4-z}$ and metallic Ag NPs. Therefore, aside from the sintering process the interplay between the species forming the above mentioned plasma plume might also lead to the formation of metallic Ag NPs and simpler metallic oxides.[55] Moreover, the presence of different Ag nanostructure morphologies could be attributed to a welding phenomenon that is a consequence of the interaction between newly created Ag NPs with further incoming fs laser pulses. As it has been extensively reported, when the distance between two or more metal NPs is sufficiently short, hybridized plasmon modes appear producing an enhancement of the near field in the interparticle gaps, reaching enough energy to melt them, which leads to the union of the nanostructures.[78,79] In addition, the non-irradiated sample was also exposed to the electron beam irradiation of the TEM and the corresponding results are presented in Fig. 9. Here, the interaction of the sample with the electron beam irradiation was completely different to that of the fs laser-irradiated sample. As soon as the electron beam interacted with Ag_2CrO_4 (Fig. 9a), the sample decomposed rapidly, forming products that adhered to the Cu–C grid of the TEM, where the sample was placed onto (Fig. 9b).

In order to understand the influence of the electron beam irradiation, a quantitative analysis was performed, as shown in Fig. 10. Fig. 10a and b display the Ag_2CrO_4 sample before and after electron beam irradiation, respectively.

The EDS characterization was performed for the two regions of Fig. 10b: region (1) already existed and region (2) formed as a consequence of the electron beam irradiation on the sample.

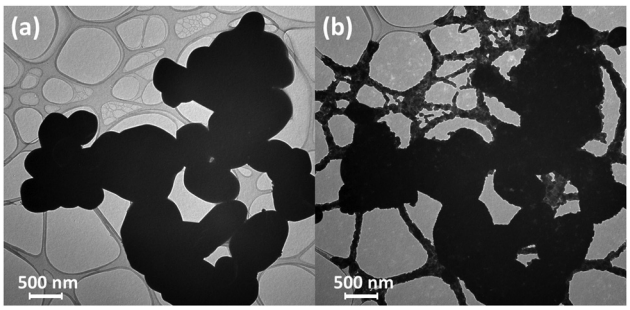

Fig. 9 TEM images of the non-irradiated Ag_2CrO_4 sample (a) before electron beam irradiation and (b) after electron beam irradiation.

As soon as the electron beam irradiation reached the sample, the formed product spread instantly along the entire Cu–C grid of the TEM. The grid worked as a template and the formed product covered the grid over a few micrometers. The EDS characterization (Fig. 10c) shows different atomic proportions of Ag (66.1% and 39.1%), Cr (30.7% and 23.0%) and O (3.2% and 37.9%) in regions 1 and 2, respectively. When we converted the elementary percentages into molar fractions to determine the stoichiometry of the products (Fig. 10e), we noticed that in both regions, the stoichiometric coefficients do not match the Ag_2CrO_4 coefficients. These results indicate that there may be other products formed by the electron beam, in addition to metallic silver, already observed.

The HR-TEM analysis displayed in Fig. 10d illustrates that the interplanar distances found in the formed product (2.58 Å and 2.59 Å) are related to the (0 4 0) plane of the orthorhombic structure of Ag_2O_3, according to the JCPDS No. 40909. Furthermore, additional values of interplanar distances were found that could not be identified as metallic Ag, Ag_2CrO_4, or simple oxides such as Ag_2O or CrO_3. This confirms our hypothesis that there are other products of unknown composition being formed simultaneously to the metallic Ag. Hence, it was neither possible to detect a proper stoichiometry for $Ag_{2-x}Cr_{1-y}O_{4-z}$ nor an estimated ratio between formed oxides and metallic Ag. This is because the amounts of Ag, Cr, and O with respect to each formed compound cannot be determined and it is not possible to distinguish the amount of metallic Ag from the total Ag amount found in the sample by using only an EDS analysis.

The Ag NP growth process and spreading through the TEM grid can be understood as a mass transport phenomenon induced by the electron beam. The atom and particle migration along the grid occurs *via* diffusion and/or convection owing to the electrical potential generated by the electron beam. When the electron beam interacts with the sample, the electrons decelerate and part of the energy dissipates *via* repeated random scattering and absorption within an interaction volume of the specimen. This energy loss, due to inelastic collisions, is mostly used in the generation of electron–hole pairs. The generated free carriers move and redistribute around the electron-irradiated region, forming relatively stable defects, also known as self-trapped excitons (STEs). The STE formation is followed by strain and bond-breaking processes that accelerate and induce

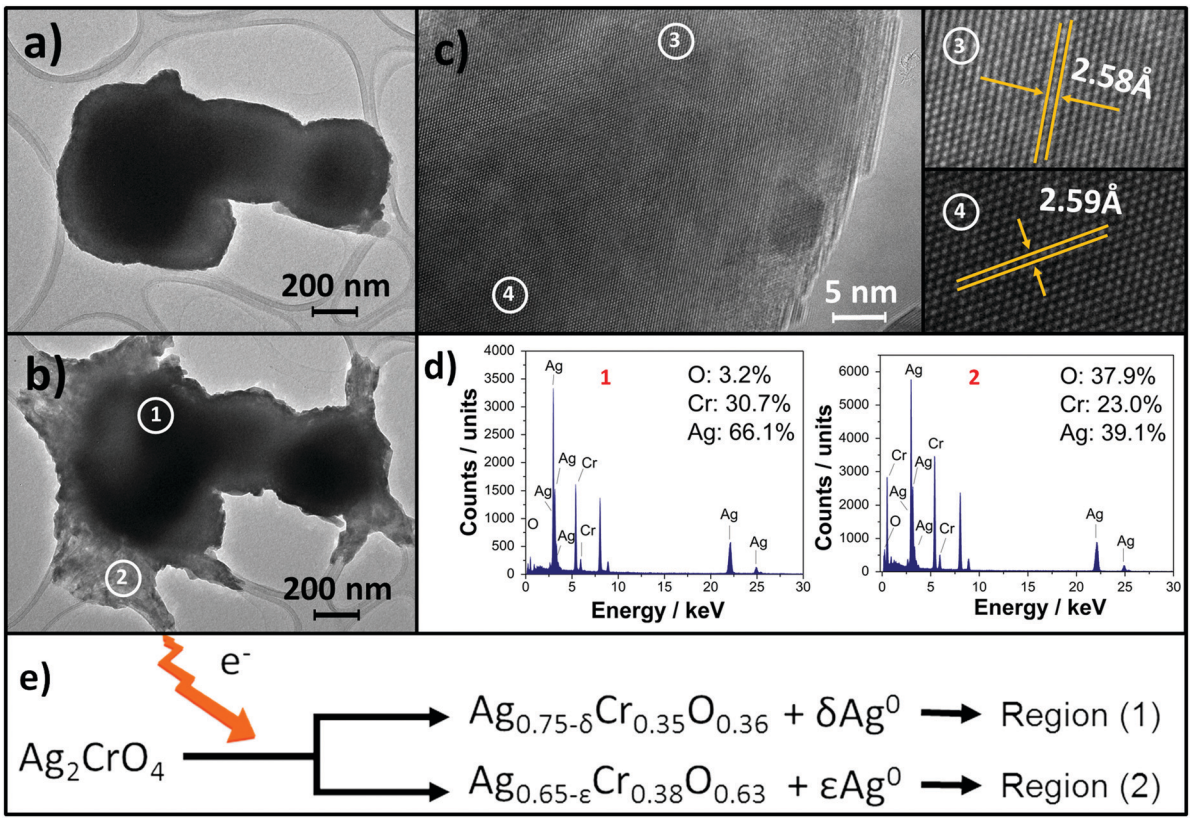

Fig. 10 TEM images (a) before electron beam irradiation and (b) after electron beam irradiation. (c) EDS characterization of the central (1) and peripheral (2) regions of the Ag_2CrO_4 microparticle and (d) high resolution TEM of an Ag_2CrO_4 microparticle.

anatomic diffusion in comparison with the environmental thermal diffusion, without electron beam irradiation.[80] The thermal energy inside the high-vacuum chamber is 7.73 million times higher than the environmental thermal energy. This condition enables a mass transport along the TEM grid.

As displayed in Fig. 3, Ag_2CrO_4 is composed of three different clusters; two of them with a predominant ionic character that act as network modifiers: $[AgO_4]$ and $[AgO_6]$; and one with a predominantly covalent character, which acts as a network former: $[CrO_4]$. We believe that the interaction between Ag_2CrO_4 and the different radiation forms, electronic or photonic, promotes the transitions of electrons from the occupied state (below the Fermi level) to the unoccupied state (usually above the Fermi level) in the oxygen atoms of the clusters. This causes an electron redistribution. Hence, stabilization of the crystal occurs, causing oxidation/reduction reactions. In this case, the clusters of Ag ($[AgO_x]$, x = 4 and 6), as constituent building blocks of Ag_2CrO_4 absorb this electronic excess, thereby reducing Ag^+ to Ag^0 and obtaining a non-stoichiometric oxide. As Ag_2CrO_4 is an n-type semiconductor, it becomes an n/p-type semiconductor at the sites where the formation of Ag^0 occurs owing to the formation of internal defects which is due to the occurrence of Ag vacancies.

The control over the growth process during fs laser or electron beam irradiation is still limited. Nevertheless, an increment in the photon/electron current typically initiates or enhances the Ag growth process, which is still localized on particular nucleation sites, where Ag is drawn from distant regions of the particles. However, the fs laser and electron beam irradiation-driven processes induce the formation of non-stoichiometric compounds and/or compounds with an unknown stoichiometry. This fact has not been observed in previous studies on similar complex semiconductor Ag_2WO_4 networks.[21,26,48,81–83]

Both products, $Ag_{2-x}Cr_{1-y}O_{4-z}$ and metallic Ag, induced by the fs laser and electron beam irradiation, are stable compounds. Their formation processes are extremely fast and deserve more profound investigations. In the future, we will investigate the effect of electron beam irradiation at cryogenic temperatures. Thus, it will be possible to determine if the mass transport occurs *via* convection or diffusion of atoms and to estimate the diffusion coefficients, which will help to understand the mass transport kinetics. Overall, these studies can provide a straightforward route for the design, iteration, and production of Ag and/or other metal NPs in semiconductor frameworks to develop promising applications.

Conclusions

The fs laser and electron beam irradiation of materials is a well-developed green process for the synthesis of metal NPs. In this study, we observed for the first time the growth of Ag NPs in Ag_2CrO_4 induced by fs laser irradiation. In addition,

we investigated the already known growth of metallic Ag in Ag_2CrO_4 induced by electron beam irradiation. The Ag_2CrO_4 sample was obtained using the precipitation method. The sample was divided into two parts; one part was irradiated with an fs laser. The XRD and micro-Raman analyses revealed that the Ag_2CrO_4 sample has an orthorhombic structure. The FE-SEM measurements showed that the non-irradiated particles present narrow size distributions (between 0.15 μm and 0.60 μm). However, the irradiated sample exhibits an expressive increase in the particle size distribution (between 0.45 μm and 2.0 μm). This result evidences the initial process of particle coalescence activated by fs laser irradiation. In addition, the TEM images reveal the presence of several micro-stems along some fs laser-irradiated particles. These micro-stems are stable and were formed during the fs laser irradiation. The non-irradiated sample reacted readily when subjected to the electron beam of the TEM. The TEM grid worked as a template and recoating took place. The EDX analysis confirms that in both irradiations, the products are formed by Ag NPs and species with unknown stoichiometry ($Ag_{2-x}Cr_{1-y}O_{4-z}$). To the best of our knowledge, the formation of Ag micro-stems induced by fs laser irradiation and the coating of a TEM grid while studying Ag_2CrO_4 are reported for the first time. These results show enormous potential for the synthesis and morphological control of Ag NPs with fs laser and electron beam irradiation. Moreover, fs laser irradiation proved to be promising for sintering studies. The electron beam irradiation results enable investigations of the growth of Ag NPs on, *e.g.*, templates or biotemplates, core–shells, or decorations.

Conflicts of interest

There are no conflicts to declare.

Acknowledgements

The authors acknowledge the financial support of agencies: CAPES (PNPD-1268069), FAPESP (2013/07296-2, 2013/26671-9), CNPq (304531/2013-8), Generalitat Valenciana for PrometeoII/2014/022, Prometeo/2016/079, ACOMP/2014/270, ACOMP/2015/1202, Ministerio de Economía y Competitividad, project CTQ2015-65207-P, MAT2016-80410-P and FIS2016-75618-R, the Ministry of Education Youth and Sports of the Czech Republic under Project No. LM2015073, the European Union for the funds Hybrid Materials for Hierarchical Structures (HyHi, Reg. No. CZ.02.1.01/0.0/0.0/16_019/0000843), to the Ministerio de Economia y Competitividad, "Salvador Madariaga" program, PRX15/00261, and finally to "Universitat Jaume I"-projects No. UJI-B2016-25, No. P11B2013-65 and UJIB-2016-38 for the financial support. The authors are also very grateful to the Serveis Centrals d'Instrumentació Científica (SCIC) of the Universitat Jaume I for the use of the femtosecond laser and microscopy facilities.

Notes and references

1 D. B. Williams and C. B. Carter, *Transmission Electron Microscopy: A Textbook for Materials Science*, 2009.
2 B. Fultz and J. Howe, *Transmission Electron Microscopy and Diffractometry of Materials*, 2013.
3 J. Xiao, P. Liu, C. X. Wang and G. W. Yang, External field-assisted laser ablation in liquid: An efficient strategy for nanocrystal synthesis and nanostructure assembly, *Prog. Mater. Sci.*, 2017, **87**, 140–220.
4 J.-G. Lee and H. Mori, Electron-irradiation-induced phase change in nanometer-sized Al_2Au particles, *Surf. Interface Anal.*, 2012, **44**, 1527–1530.
5 N. Ali, S. Bashir, I. K. Umm, N. Begum and T. Hussain, Study of variation in surface morphology, chemical composition, crystallinity and hardness of laser irradiated silver in dry and wet environments, *Opt. Laser Technol.*, 2017, **92**, 173–181.
6 P. A. Sheena, K. P. Prianka, N. A. Sabu, S. Ganesh and T. Varghese, Effect of electron beam irradiation on the structure and optical properties of nickel oxide nanocubes, *Bull. Mater. Sci.*, 2015, **38**, 825–830.
7 V. D. Frolov, P. A. Pivovarov, E. V. Zavedeev and V. I. Konov, Influence of laser irradiation on local electronic properties of graphene in the presence of water adsorbate, *Opt. Laser Technol.*, 2017, **90**, 216–221.
8 D. Fang, X. Fang, Y. Li, B. Yao, H. Zhao, Z. Wei, J. Tang, C. Du, J. Li, X. Ma, D. D. Wang and Y. S. Yan, Photoluminescence Properties of the GaSb Nanostructures Irradiated by Femtosecond Laser, *Nanosci. Nanotechnol. Lett.*, 2015, **7**, 117–120.
9 W. Zhao, J. Zhang, J. Pan, J. Qiu, J. Niu and C. Li, One-step electrospinning route of SrTiO(3)-modified Rutile TiO(2)nanofibers and its photocatalytic properties, *Nanoscale Res. Lett.*, 2017, **12**, 371.
10 V. M. Longo, C. C. De Foggi, M. M. Ferrer, A. F. Gouveia, R. S. André, W. Avansi, C. E. Vergani, A. L. Machado, J. Andrés, L. S. Cavalcante, A. C. Hernandes and E. Longo, Potentiated Electron Transference in α-Ag_2WO_4 Microcrystals with Ag Nanofilaments as Microbial Agent, *J. Phys. Chem. A*, 2014, **118**, 5769–5778.
11 J. Andrés, E. Longo, A. F. Gouveia, J. P. C. Costa, L. Gracia and M. C. Oliveira, *In situ* Formation of Metal Nanoparticles through Electron Beam Irradiation: Modeling Real Materials from First-Principles Calculations, *J. Mater. Sci. Eng.*, 2018, **7**, 461.
12 J. Hu, Y. Sun and Z. Chen, Rapid Fabrication of Nanocrystals through in situ Electron Beam Irradiation in a Transmission Electron Microscope, *J. Phys. Chem. C*, 2009, **113**, 5201–5205.
13 I. G. Gonzalez-Martinez, A. Bachmatiuk, V. Bezugly, J. Kunstmann, T. Gemming, Z. Liu, G. Cuniberti and M. H. Rummeli, Electron-beam induced synthesis of nanostructures: a review, *Nanoscale*, 2016, **8**, 11340–11362.
14 J. Do, M. Fedoruk, F. Jäckel and J. Feldmann, Two-Color Laser Printing of Individual Gold Nanorods, *Nano Lett.*, 2013, **13**, 4164–4168.

15 M. A. Huergo, C. M. Maier, M. F. Castez, C. Vericat, S. Nedev, R. C. Salvarezza, A. S. Urban and J. Feldmann, Optical Nanoparticle Sorting Elucidates Synthesis of Plasmonic Nanotriangles, *ACS Nano*, 2016, **10**, 3614–3621.

16 M. J. Guffey, R. L. Miller, S. K. Gray and N. F. Scherer, Plasmon-Driven Selective Deposition of Au Bipyramidal Nanoparticles, *Nano Lett.*, 2011, **11**, 4058–4066.

17 S. S. Chou, B. S. Swartzentruber, M. T. Janish, K. C. Meyer, L. B. Biedermann, S. Okur, D. B. Burckel, C. B. Carter and B. Kaehr, Laser Direct Write Synthesis of Lead Halide Perovskites, The, *J. Phys. Chem. Lett.*, 2016, **7**, 3736–3741.

18 D. Tan, K. N. Sharafudeen, Y. Yue and J. Qiu, Femtosecond laser induced phenomena in transparent solid materials: Fundamentals and applications, *Prog. Mater. Sci.*, 2016, **76**, 154–228.

19 D. Zhang, B. Gökce and S. Barcikowski, Laser Synthesis and Processing of Colloids: Fundamentals and Applications, *Chem. Rev.*, 2017, **117**, 3990–4103.

20 J. Andrés, L. Gracia, P. Gonzalez-Navarrete, V. M. Longo, W. Avansi Jr., D. P. Volanti, M. M. Ferrer, P. S. Lemos, F. A. La Porta, A. C. Hernandes and E. Longo, Structural and electronic analysis of the atomic scale nucleation of Ag on α-Ag_2WO_4 induced by electron irradiation, *Sci. Rep.*, 2014, **4**, 5391.

21 R. A. Roca, A. F. Gouveia, P. S. Lemos, L. Gracia, J. Andrés and E. Longo, Formation of Ag Nanoparticles on β-Ag_2WO_4 through Electron Beam Irradiation: A Synergetic Computational and Experimental Study, *Inorg. Chem.*, 2016, **55**, 8661–8671.

22 M. Umalas, S. Vlassov, B. Polyakov, L. M. Dorogin, R. Saar, I. Kink, R. Lõhmus, A. Lõhmus and A. E. Romanov, Electron beam induced growth of silver nanowhiskers, *J. Cryst. Grow.*, 2015, **410**, 63–68.

23 Y. Makita, O. Ikai, A. Ookubo and K. Ooi, Preparation of Long Silver Nanowires from Silver Matrix by Electron Beam Irradiation, *Chem. Lett.*, 2002, 928–929.

24 M. Edmondson, W. Z. Zhou, S. A. Sieber, I. Jones, I. Gameson, P. A. Anderson and P. Edwards, *Electron-Beam Induced Growth of Bare Silver Nanowires from Zeolite Crystallites*, 2001, vol. 13.

25 M. Pattabi, R. M. Pattabi and G. Sanjeev, *Studies on the growth and stability of silver nanoparticles synthesized by electron beam irradiation*, 2009, vol. 20.

26 R. Alvarez Roca, P. S. Lemos, J. Andrés and E. Longo, Formation of Ag nanoparticles on metastable β-Ag_2WO_4 microcrystals induced by electron irradiation, *Chem. Phys. Lett.*, 2016, **644**, 68–72.

27 Z.-Y. Yuan, W. Zhou, V. Parvulescu and B.-L. Su, Electron beam irradiation effect on nanostructured molecular sieve catalysts, *J. Electron Spectrosc. Relat. Phenom.*, 2003, **129**, 189–194.

28 K. Li and F.-S. Zhang, *A novel approach for preparing silver nanoparticles under electron beam irradiation*, 2009, vol. 12.

29 C. Ma, X. Chen, X. Tan, P. Hu, Q. Li, Y. Cao and X. Liang, In situ fabrication of silver-based nanostructures using electron beam, *CrystEngComm*, 2018, **20**, 2227–2232.

30 J.-U. Kim, S.-H. Cha, K. Shin, J. Y. Jho and J.-C. Lee, Synthesis of Gold Nanoparticles from Gold(I)–Alkanethiolate Complexes with Supramolecular Structures through Electron Beam Irradiation in TEM, *J. Am. Chem. Soc.*, 2005, **127**, 9962–9963.

31 A. Imanishi, M. Tamura and S. Kuwabata, Formation of Au nanoparticles in an ionic liquid by electron beam irradiation, *Chem. Commun.*, 2009, 1775–1777.

32 S. K. Mahapatra, K. A. Bogle, S. D. Dhole and V. N. Bhoraskar, Synthesis of gold and silver nanoparticles by electron irradiation at 5–15 keV energy, *Nanotechnology*, 2007, **18**, 135602.

33 S. Sepulveda-Guzman, N. Elizondo-Villarreal, D. F. A. Torres-Castro, X. Gao, J. P. Zhou and M. J. Yacaman, *In situ* formation of bismuth nanoparticles through electron-beam irradiation in a transmission electron microscope, *Nanotechnology*, 2007, **18**, 335604.

34 G. Constantinescu, S. Rasekh, M. A. Torres, P. Bosque, M. A. Madre, A. Sotelo and J. C. Diez, Thermoelectric doping effect in $Ca_3Co_{4-x}Ni_xO_9$ ceramics, *Bol. Soc. Esp. Ceram. Vidrio*, 2015, **54**, 21–27.

35 A. Pitto-Barry, L. M. A. Perdigao, M. Walker, J. Lawrence, G. Costantini, P. J. Sadler and N. P. E. Barry, Synthesis and controlled growth of osmium nanoparticles by electron irradiation, *Dalton Trans.*, 2015, **44**, 20308–20311.

36 J. M. P. Almeida, L. De Boni, W. Avansi, C. Ribeiro, E. Longo, A. C. Hernandes and C. R. Mendonca, Generation of copper nanoparticles induced by fs-laser irradiation in borosilicate glass, *Opt. Express*, 2012, **20**, 15106–15113.

37 P. A. Anderson, M. Edmondson, P. Edwards, I. Gameson, P. Jill Meadows, S. Johnson and W. Zhou, *Production of Ultrafine Single-Crystal Copper Wires through Electron Beam Irradiation of Cu-containing Zeolite X*, 2005, vol. 631.

38 E. U. Donev, G. Schardein, J. C. Wright and J. Todd Hastings, *Substrate effects on the electron-beam-induced deposition of platinum from a liquid precursor*, 2011, vol. 3.

39 J. Ghatak, W. Guan and G. Mobus, *In situ* TEM observation of lithium nanoparticle growth and morphological cycling, *Nanoscale*, 2012, **4**, 1754–1759.

40 W. Neng, L.-T. Sun, X.-H. Hu, Y.-Y. Zhu, Z. Lin, X. Tao, H.-C. Bi, S. Jun and F.-Z. Dong, Charge Supported Growth and Superplasticity of Sodium Nanostructures, *Cryst. Growth Des.*, 2012, **12**, 3899–3905.

41 E. S. Bochkareva, A. I. Sidorov, U. V. Yurina and O. A. Podsvirov, Formation of metal nanoparticles in MgF_2, CaF_2 and BaF_2 crystals under the electron beam irradiation, *Nucl. Instrum. Methods Phys. Res., Sect. B*, 2017, **403**, 1–6.

42 S. Rix, U. Natura, F. Loske, M. Letz, C. Felser, M. Reichling, S. Rix, U. Natura, F. Loske, M. Letz and C. Felser, Formation of metallic colloids in CaF_2 by intense ultraviolet light, *Appl. Phys. Lett.*, 2011, **99**, 261909.

43 P. T. Anastas and J. C. Warner, *Green Chemistry: Theory and Practice*, 2000, vol. 30.

44 S. Ma, X. Chen, B. Zhao, H. Dong, Q. Yuan, L. Li, J. Lv, L. Shi and L. Chen, Facile preparation of a silver nanoparticles-containing membrane with an enhanced catalysis and separation, *Appl. Catal., A*, 2017, **536**, 35–44.

45 L. F. da Silva, A. C. Catto, W. Avansi, L. S. Cavalcante, V. R. Mastelaro, J. Andrés, K. Aguir and E. Longo, Acetone gas sensor based on α-Ag_2WO_4 nanorods obtained via a microwave-assisted hydrothermal route, *J. Alloys Compd.*, 2016, **683**, 186–190.

46 R. A. Roca, J. C. Sczancoski, I. C. Nogueira, M. T. Fabbro, H. C. Alves, L. Gracia, L. P. S. Santos, C. P. de Sousa, J. Andres, G. E. Luz, E. Longo and L. S. Cavalcante, Facet-dependent photocatalytic and antibacterial properties of α-Ag_2WO_4 crystals: combining experimental data and theoretical insights, *Catal. Sci. Technol.*, 2015, **5**, 4091–4107.

47 P. S. Lemos, A. Altomare, A. F. Gouveia, I. C. Nogueira, L. Gracia, R. Llusar, J. Andres, E. Longo and L. S. Cavalcante, Synthesis and characterization of metastable β-Ag_2WO_4: an experimental and theoretical approach, *Dalton Trans.*, 2016, **45**, 1185–1191.

48 R. A. Roca, P. S. Lemos, L. Gracia, J. Andres and E. Longo, Uncovering the metastable γ-Ag_2WO_4 phase: a joint experimental and theoretical study, *RSC Adv.*, 2017, **7**, 5610–5620.

49 M. T. Fabbro, C. Saliby, L. R. Rios, F. A. La Porta, L. Gracia, M. S. Li, J. Andrés, L. P. S. Santos and E. Longo, Identifying and rationalizing the morphological, structural, and optical properties of -Ag(2)MoO(4) microcrystals, and the formation process of Ag nanoparticles on their surfaces: combining experimental data and first-principles calculations, *Sci. Technol. Adv. Mater.*, 2015, **16**, 65002.

50 G. Botelho, J. C. Sczancoski, J. Andres, L. Gracia and E. Longo, Experimental and Theoretical Study on the Structure, Optical Properties, and Growth of Metallic Silver Nanostructures in Ag_3PO_4, *J. Phys. Chem. C*, 2015, **119**, 6293–6306.

51 T. Yan, W. Guan, Y. Xiao, J. Tian, Z. Qiao, H. Zhai, W. Li and J. You, Effect of thermal annealing on the microstructures and photocatalytic performance of silver orthophosphate: The synergistic mechanism of Ag vacancies and metallic Ag, *Appl. Surf. Sci.*, 2017, **391**, 592–600.

52 R. C. de Oliveira, M. Assis, M. M. Teixeira, M. D. P. da Silva, M. S. Li, J. Andres, L. Gracia and E. Longo, An Experimental and Computational Study of β-$AgVO_3$: Optical Properties and Formation of Ag Nanoparticles, *J. Phys. Chem. C*, 2016, **120**, 12254–12264.

53 M. T. Fabbro, L. Gracia, G. S. Silva, L. P. S. Santos, J. Andrés, E. Cordoncillo and E. Longo, Understanding the formation and growth of Ag nanoparticles on silver chromate induced by electron irradiation in electron microscope: A combined experimental and theoretical study, *J. Solid State Chem.*, 2016, **239**, 220–227.

54 A. Mansourian, S. A. Paknejad, A. V. Zayats and S. H. Mannan, Stereoscopic Nanoscale-Precision Growth of Free-Standing Silver Nanorods by Electron Beam Irradiation, *J. Phys. Chem. C*, 2016, **120**, 20310–20314.

55 M. Assis, E. Cordoncillo, R. Torres-Mendieta, H. Beltrán-Mir, G. Mínguez-Vega, R. Oliveira, E. R. Leite, C. C. Foggi, C. E. Vergani, E. Longo and J. Andrés, Towards the scale-up of the formation of nanoparticles on α-Ag_2WO_4 with bactericidal properties by femtosecond laser irradiation, *Sci. Rep.*, 2018, **8**, 1884.

56 M. Assis, E. Cordoncillo, R. Torres-Mendieta, H. Beltran-Mir, G. Minguez-Vega, A. F. Gouveia, E. Leite, J. Andres and E. Longo, Laser-induced formation of bismuth nanoparticles, *Phys. Chem. Chem. Phys.*, 2018, **20**, 13693–13696.

57 M. Assis, N. G. Macedo, T. R. Machado, M. M. Ferrer, A. F. Gouveia, E. Cordoncillo, R. Torres-Mendieta, H. Beltrán-Mir, G. Mínguez-Vega, E. R. Leite, J. R. Sambrano, J. Andrés and E. Longo, Laser/Electron Irradiation on Indium Phosphide (InP) Semiconductor: Promising Pathways to In Situ Formation of Indium Nanoparticles, *Part. Part. Syst. Charact.*, 2018, **35**, 1800237.

58 S. Ouyang, Z. Li, Z. Ouyang, T. Yu, J. Ye and Z. Zou, Correlation of Crystal Structures, Electronic Structures, and Photocatalytic Properties in a Series of Ag-based Oxides: $AgAlO_2$, $AgCrO_2$, and Ag_2CrO_4, *J. Phys. Chem. C*, 2008, **112**, 3134–3141.

59 R. F. Alamdari, S. S. Hajimirsadeghi and I. Kohsari, Synthesis of silver chromate nanoparticles: Parameter optimization using Taguchi design, *Inorg. Mater.*, 2010, **46**, 60–64.

60 Y. Liu, H. Yu, M. Cai and J. Sun, Microwave hydrothermal synthesis of Ag_2CrO_4 photocatalyst for fast degradation of PCP-Na under visible light irradiation, *Catal. Commun.*, 2012, **26**, 63–67.

61 F. Soofivand, F. Mohandes and M. Salavati-Niasari, Silver chromate and silver dichromate nanostructures: Sonochemical synthesis, characterization, and photocatalytic properties, *Mater. Res. Bull.*, 2013, **48**, 2084–2094.

62 J. Shen, Y. Lu, J.-K. Liu and X.-H. Yang, Photocatalytic activity of silver chromate materials by various synthesis methods, *J. Exp. Nanosci.*, 2016, **11**, 650–659.

63 D. Xu, B. Cheng, J. Zhang, W. Wang, J. Yu and W. Ho, Photocatalytic activity of Ag_2MO_4 (M = Cr, Mo, W) photocatalysts, *J. Mater. Chem. A*, 2015, **3**, 20153–20166.

64 J. Zhang, W. Yu, J. Liu and B. Liu, Illustration of high-active Ag_2CrO_4 photocatalyst from the first-principle calculation of electronic structures and carrier effective mass, *Appl. Surf. Sci.*, 2015, **358**, 457–462.

65 D. Xu, S. Cao, J. Zhang, B. Cheng and J. Yu, Effects of the preparation method on the structure and the visible-light photocatalytic activity of Ag_2CrO_4, *Beilstein J. Nanotechnol.*, 2014, **5**, 658–666.

66 G. S. Silva, L. Gracia, M. T. Fabbro, L. P. S. Santos, H. Beltrán-Mir, E. Cordoncillo, E. Longo and J. Andrés, Theoretical and Experimental Insight on Ag_2CrO_4 Microcrystals: Synthesis, Characterization, and Photoluminescence Properties, *Inorg. Chem.*, 2016, **55**, 8961–8970.

67 E. Longo, D. P. Volanti, V. M. Longo, L. Gracia, I. C. Nogueira, M. A. P. Almeida, A. N. Pinheiro, M. M. Ferrer, L. S. Cavalcante and J. Andrés, Toward an Understanding of the Growth of Ag Filaments on α-Ag_2WO_4 and Their Photoluminescent Properties: A Combined Experimental and Theoretical Study, *J. Phys. Chem. C*, 2014, **118**, 1229–1239.

68 T. Atsuhiro, H. Keiji and K. Hiroshi, Control of Surface Plasmon Resonance of Au/SnO_2 by Modification with Ag and Cu for Photoinduced Reactions under Visible-Light Irradiation over a Wide Range, *Chem. – Eur. J.*, 2016, **22**, 4592–4599.

69 S. S. Patil, D. R. Patil, S. K. Apte, M. V. Kulkarni, J. D. Ambekar, C.-J. Park, S. W. Gosavi, S. S. Kolekar and B. B. Kale, Confinement of Ag_3PO_4 nanoparticles supported by surface plasmon resonance of Ag in glass: Efficient nanoscale photocatalyst for solar H_2 production from waste H_2S, *Appl. Catal., B*, 2016, **190**, 75–84.

70 M. L. Hackert and R. A. Jacobson, The crystal structure of silver chromate, *J. Solid State Chem.*, 1971, **3**, 364–368.

71 M. T. Fabbro, C. C. Foggi, L. P. S. Santos, L. Gracia, A. Perrin, C. Perrin, C. E. Vergani, A. L. Machado, J. Andres, E. Cordoncillo and E. Longo, Synthesis, antifungal evaluation and optical properties of silver molybdate microcrystals in different solvents: a combined experimental and theoretical study, *Dalton Trans.*, 2016, **45**, 10736–10743.

72 D. Santamaría-Pérez, E. Bandiello, D. Errandonea, J. Ruiz-Fuertes, O. Gomis, J. A. Sans, F. J. Manjón, P. Rodríguez-Hernández and A. Muñoz, Phase Behaviour of Ag_2CrO_4 under Compression: Structural, Vibrational, and Optical Properties, *J. Phys. Chem. C*, 2013, **117**, 12239–12248.

73 X. Zhang, Z. Shen, J. Liu, S. N. Kerisit, M. E. Bowden, M. L. Sushko, J. J. De Yoreo and K. M. Rosso, Direction-specific interaction forces underlying zinc oxide crystal growth by oriented attachment, *Nat. Commun.*, 2017, **8**, 835.

74 R. M. German, Coarsening in Sintering: Grain Shape Distribution, Grain Size Distribution, and Grain Growth Kinetics in Solid-Pore Systems, *Crit. Rev. Solid State Mater. Sci.*, 2010, **35**, 263–305.

75 R. Ebert, F. Ullmann, D. Hildebrandt, J. Schille, L. Hartwig, S. Kloetzer, A. Streek and H. Exner, Laser Processing of Tungsten Powder with Femtosecond Laser Radiation, *J. Laser Micro/Nanoeng.*, 2012, **7**, 38–43.

76 V. Amendola and M. Meneghetti, What controls the composition and the structure of nanomaterials generated by laser ablation in liquid solution?, *Phys. Chem. Chem. Phys.*, 2013, **15**, 3027–3046.

77 S. W. Sofie, P. Gannon and V. Gorokhovsky, Silver-chromium oxide interactions in SOFC environments, *J. Power Sources*, 2009, **191**, 465–472.

78 G. González-Rubio, J. González-Izquierdo, L. Bañares, G. Tardajos, A. Rivera, T. Altantzis, S. Blas, O. Peña-Rodríguez, A. Guerrro-Martínez and L. M. Liz-Marzán, Femtosecond laser-controlled tip-to-tip assembly and welding of gold nanorods, *Nano Lett.*, 2015, **15**, 8282–8288.

79 G. González-Rubio, A. Guerrero-Martínez and L. M. Liz-Marzán, Reshaping, fragmentation, and assembly of gold nanoparticles assisted by pulse lasers, *Acc. Chem. Res.*, 2016, **49**, 678–686.

80 C. Cserhati, S. Charnovych, P. M. Lytvyn, M. L. Trunov, D. L. Beke, Y. Kaganovskii and S. Kökényesi, E-beam induced mass transport in amorphous $As_{20}Se_{80}$ films, *Mater. Lett.*, 2012, **85**, 113–116.

81 M. A. San-Miguel, E. Z. da Silva, S. M. Zanetti, M. Cilense, M. T. Fabbro, L. Gracia, J. Andrés and E. Longo, In situ growth of Ag nanoparticles on α-Ag_2WO_4 under electron irradiation: probing the physical principles, *Nanotechnology*, 2016, **27**, 225703.

82 E. Longo, L. S. Cavalcante, D. P. Volanti, A. F. Gouveia, V. M. Longo, J. A. Varela, M. O. Orlandi and J. Andrés, Direct *in situ* observation of the electron-driven synthesis of Ag filaments on α-Ag(2)WO(4) crystals, *Sci. Rep.*, 2013, **3**, 1676.

83 W. da, S. Pereira, J. Andres, L. Gracia, M. A. San-Miguel, E. Z. da Silva, E. Longo and V. M. Longo, Elucidating the real-time Ag nanoparticle growth on α-Ag_2WO_4 during electron beam irradiation: experimental evidence and theoretical insights, *Phys. Chem. Chem. Phys.*, 2015, **17**, 5352–5359.